HHS Public Access

Author manuscript

Nat Photonics. Author manuscript; available in PMC 2015 March 01.

Published in final edited form as:

Nat Photonics. 2014 September 1; 8: 710–715. doi:10.1038/nphoton.2014.165.

High-throughput optical screening of cellular mechanotransduction

Jonathan L. Compton[1,2], **Justin C. Luo**[2,3], **Huan Ma**[1,2], **Elliot Botvinick**[2,3,4,*], and **Vasan Venugopalan**[1,2,3,*]

[1] Department of Chemical Engineering and Materials Science, University of California, Irvine

[2] Laser Microbeam and Medical Program, Beckman Laser Institute, University of California, Irvine

[3] Department of Biomedical Engineering, University of California, Irvine

[4] Edwards Lifesciences Center for Advanced Cardiovascular Technology, University of California, Irvine

Abstract

We introduce an optical platform for rapid, high-throughput screening of exogenous molecules that affect cellular mechanotransduction. Our method initiates mechanotransduction in adherent cells using single laser-microbeam generated micro-cavitation bubbles (μCBs) without requiring flow chambers or microfluidics. These μCBs expose adherent cells to a microTsunami, a transient microscale burst of hydrodynamic shear stress, which stimulates cells over areas approaching 1mm^2. We demonstrate microTsunami-initiated mechanosignalling in primary human endothelial cells. This observed signalling is consistent with G-protein-coupled receptor stimulation resulting in Ca^{2+} release by the endoplasmic reticulum. Moreover, we demonstrate the dose-dependent modulation of microTsunami-induced Ca^{2+} signalling by introducing a known inhibitor to this pathway. The imaging of Ca^{2+} signalling, and its modulation by exogenous molecules, demonstrates the capacity to initiate and assess cellular mechanosignalling in real-time. We utilize this capability to screen the effects of a set of small molecules on cellular mechanotransduction in 96-well plates using standard imaging cytometry.

Background and Introduction

Mechanical forces resulting from cell-cell and cell-matrix interactions are known to influence cell signalling[1], function[2], homeostasis[3], and fate[4] in individual cells and cell populations[5] via the process of mechanotransduction whereby mechanical stimuli are converted to biochemical activity. At the cellular level, these processes are mediated by specialized force-sensitive molecules such as stretch-activated ion-channels, receptor tyrosine kinases, junction proteins and integrins[6]. The results of numerous studies support

* Corresponding Authors: ebotvini@uci.edu, vvenugop@uci.edu.

Author Contributions: ELB and VV conceived the project. JLC, JCL, ELB, VV designed the experiments. JLC, JCL and HM performed the experiments. JLC and VV developed the hydrodynamic model. JLC, JCL, ELB, and VV performed the data analysis. JLC, JCL, ELB, and VV wrote the paper.

the important role of mechanotransduction in many vital processes including tissue morphogenesis, stem cell differentiation, vascular regulation, and tumour metastasis[7]. Moreover, there is mounting evidence that disruptive mechanical cues and/or dysregulation of mechanotransduction pathways play important roles in the initiation and/or progression of numerous diseases including atrial fibrillation, hypertension, osteoporosis, digestive diseases, and cancer[7–10]. This evidence has raised awareness for the need to develop drug discovery assays that incorporate the sensitivity of candidate drug targets to mechanosignalling[11,12]. This heightened awareness is spurring vigorous efforts to discover molecules that modulate cellular mechanotransduction activity[13–15]. We postulate the existence of classes of 'mechano-active' drugs that can target these pathways; drugs that remain undiscovered because there is no practical method to implement high-throughput screening (HTS).

Currently, there are several established, high-throughput methods to precisely measure changes in cellular activity including imaging cytometry and gene arrays[14]. However, precise mechanical stimulation of cells is non-trivial and requires specialized techniques such as atomic force microscopy, optical/magnetic tweezers, dynamically-stretched substrates or laminar flow chambers[1,16–21]. These methods are not standardized and they are incompatible with existing high-throughput drug discovery platforms.

Approach

Here we report the development and demonstration of an optical platform (Fig. 1) that combines: (a) pulsed laser irradiation for the generation of single *microcavitation bubbles* (μCBs) to provide precise mechanical stimulation of many adherent cells with (b) dynamic fluorescence imaging for real-time high-throughout measurement of cellular signalling. A μCB is produced through the precise delivery of a single focused laser pulse (pulsed laser microbeam) 10μm above an adherent cell culture. The displacement of aqueous media due to the dynamic expansion and collapse of the μCB exposes the cells to a *microTsunami*: a transient burst of hydrodynamic shear stress with highly controllable location, amplitude, duration, and spatial extent[22,23] (Fig. 2). The microTsunami (μTsunami) shear stress exposures are typically microseconds long and can be tuned in duration and amplitude to provide sub- and supra-physiological shear stress impulses in regions as large as 1 mm in diameter (Fig. 2). In previous studies, we established that, in adherent cell cultures, the laser-generated μTsunami produces hydrodynamic shear stresses that can cause cell lysis, necrosis, and molecular delivery in well-defined spatial regions proximal to the μCB[22,23]. Here we demonstrate that such μTsunamis also have the capacity to initiate mechanotransduction signalling in adherent cells located in regions extending far beyond both the zone of cellular injury and maximum μCB size. The application of tailored hydrodynamic stresses in this fashion, combined with the use of imaging cytometry, provides an immediate readout of the responsiveness of an entire cell population to external mechanical stimuli.

To examine the cellular response to these laser-generated μTsunamis, we employed a classical model system of vascular mechanotransduction[24] in which the release of Ca^{2+} ions from the endoplasmic reticulum (ER) of primary Human Umbilical Vein Endothelial Cells

(HUVECs) is monitored fluorescently. Intracellular calcium regulates processes downstream of mechanotransduction in HUVECs including the production of nitric oxide (NO)[25,26]. Given the prominent role that mechanotransduction plays in the cardiovascular system, primary HUVEC culture provides an ideal context in which to test our μTsunami platform. Below we demonstrate our ability to stimulate a mechanotransduction pathway using μTsunamis and to alter that pathway's sensitivity to hydrodynamic stresses using a known chemical inhibitor. For these studies, we cultured HUVECs on glass bottom Petri dishes and labelled them with Fluo-3/AM, a fluorescent reporter whose emission increases upon binding to cytoplasmic Ca^{2+}. Culture media was replaced with Ca^{2+}-free media for the μTsunami experiments. This media was supplemented with 3mM EGTA, to ensure chelation of extracellular Ca^{2+} ions[27,28]. Thus, any observed Ca^{2+} signalling originates from intracellular stores and not from Ca^{2+} transport across plasma membrane ion channels.

The μCBs are produced in aqueous cell culture via optical breakdown. Optical breakdown is the formation of a laser-induced plasma that is typically initiated through a combination of multi-photon and cascade ionization processes[29–31]. The absorption of the laser microbeam radiation by the plasma leads to vaporization of the aqueous medium within the laser microbeam focal volume resulting in μCB formation. Thus while the optical breakdown event is typically confined to the focal region with characteristic sub-micrometre dimensions (depending on optical parameters), the resulting μCB diameter can range from less than a micrometre to a few millimetres. Optical breakdown initiated cavitation has been extensively studied and employed for biomedical applications ranging from laser lithotripsy and intraocular microsurgery to targeted lysis and molecular delivery to adherent cells[22,23,30,32,33].

We implemented the Gilmore model[34,35] to predict the μCB dynamics and resulting cellular exposure to hydrodynamic stresses. The Gilmore model has been used extensively to model cavitation bubbles dynamics; including those generated by pulsed laser microbeam irradiation[36-38]. This model provides quantitative predictions (see Methods) for the time-resolved bubble wall radius $R_B(t)$ and velocity $V_B(t)$ (Fig. 2a). Time-resolved imaging of laser-generated μCBs has successfully verified the accuracy of Gilmore model predictions[37,38]. Importantly, once the maximum bubble size and fluid medium is specified, the μCB dynamics are uniquely determined. Because the μCB is responsible for the fluid displacement, the maximum μCB radius R_{max} alone determines the cellular exposure to the hydrodynamic stresses. Thus by using a single pulsed laser microbeam exposure, we can generate a μTsunami that provides a tailored exposure of hydrodynamic shear stress to an adherent cell culture. Below we show that μTsunamis can induce cellular mechanosignalling within primary HUVEC cultures and demonstrate modulation of this cellular response using a known chemical inhibitor of mechanotransduction. We further demonstrate the use of this approach to perform a high-throughput screen of cellular mechanotransduction under nine different conditions in a 96-well plate.

Results

In Fig. 2a we plot the time-resolved shear stress at radial locations r_1=150 μm and r_2=300 μm generated by a μCB with R_{max}=108 μm, which is identical to that used in the

experimental study. As would be expected intuitively, the Gilmore model predicts a reduction in the maximum fluid shear stress with increasing radial distance from the bubble centre. While the maximum stresses can be several orders of magnitude larger than physiological shear stresses in the circulatory system, they only persist over microsecond time scales. We can determine the local cellular exposure to the shear stress impulse produced by the μTsunami by integrating the local time-resolved shear stress over the entire μCB cycle. This impulse is particularly relevant, as it has been shown to provide a quantitative metric that predicts cellular necrosis and molecular delivery in regions proximal to the μCB[38]. Impulse is plotted as a function of radial distance in Fig. 2b. The calculated impulse values are below those experienced physiologically by human vascular endothelial cells (0.1-10 Pa s)[39] and can be easily tuned by varying the μCB diameter.

Experimentally, we determined that the delivery of a single 5μJ pulsed laser microbeam generated μCBs with R_{max} =108 μm initiates Ca^{2+} signalling of cultured primary HUVEC cultures. The signalling probability and dynamics is dependent upon cell position relative to the μCB centre (Fig. 3a). For example, cells located at distances of approximately 60, 150, and 240 μm from the μCB centre show increasing delays, on the order of many seconds, in the initiation of signalling (Fig. 3b). Such latency in the ER response to high shear stress has been reported in Ca^{2+}-free culture conditions[28]. In fact, we found a systematic increase in signalling delay time with radial distance from the μCB centre (Fig. 3c), where the speed of this Ca^{2+} wave can be estimated from the slope of a linear regression as 4.5 ± 0.3 μm/s (95% confidence interval).Interestingly, even cells immediately adjacent to the site of laser microbeam delivery have signalling delays of several seconds following the expansion and collapse of the μCB, which occurs within 20 μs. Taken together, these results are consistent with a hypothesis that the available concentration of a diffusible intracellular mediator within each cell is modulated by the magnitude of the locally applied shear stress impulse. The intracellular transport of such a mediator would result in both the observed increasing signalling delays and decreasing signalling probabilities with increasing distance from the μCB centre (Fig. 3d). The low signalling probability observed for cells nearest to the μCB is likely due to cell lysis or transient membrane permeabilization as supported by our previous work[22,23,38]. At larger distances we observe a monotonic relationship between the decreasing shear stress impulse and Ca^{2+} signalling probability. In support of our signalling probability data, we close each experiment by dosing cells with 50 μM ATP (data not shown) to confirm that the cells remain responsive to chemical stimulation of ER Ca^{2+} release.

For our system to be useful in HTS we must demonstrate sensitivity to changes in mechanosignalling with the addition of a putative inhibitor. We postulated that μTsunami exposure, either directly or indirectly, stimulates G-protein coupled receptors at the apical surface, which in turn leads to the production of Inositol trisphosphate (IP_3) that diffuses to the ER where it binds the IP_3 receptor and stimulates Ca^{2+} release. We repeated our assay in the presence of 2-Aminoethoxy-diphenyl borate (2-APB) which inhibits IP_3-induced Ca^{2+} release[28, 40], by competitively binding the IP_3 receptor. HUVECs were cultured to confluence and incubated with 2-APB at concentrations of 10 μM, 30 μM or 100 μM, previously shown to provide dose-dependent inhibition of Ca^{2+} release following

stimulation using a bolus of ATP[40]. We found that 2-APB attenuates the spatial and temporal extent of μTsunami-induced Ca^{2+} signalling in a dose-dependent manner (Fig. 4a). Fig. 4b summarizes results from many trials and quantifies the attenuation of both the signalling probability and spatial extent with increasing 2-APB concentration and decreasing shear stress impulse.

To support our assertion that this approach can be used in HTS, we performed experiments in a 96-well plate to test the effects of seven different molecules, each with eight or sixteen replicates: (i, ii) 10 μM and 100 μM 2-APB; (iii) 10 μM PP2 (phosphoprotein phosphatase 2), a known Src family kinase inhibitor; (iv) 50 nM Verapamil, a voltage-dependent calcium channel blocker used to treat hypertension; (v) 10 μM cytochalasin-D, an inhibitor of actin polymerization; (vi) 20 μM nocodazole, an inhibitor of microtubule polymerization; and (vii) 20 μM blebbistatin, an inhibitor of non-muscle myosin-IIA. As controls, we measured μTsunami-induced Ca^{2+} signalling in (a) Ca^{2+}-free culture media alone and in (b) Ca^{2+}-free culture media plus 5% DMSO.

Figure 5 summarizes results of the screen by reporting the percentage of cells in each well located within a 100-150 μm annular ring surrounding the μCB centre that exhibits μTsunami-induced Ca^{2+} signalling. The median value for the percentage of activated cells in each of the nine groups is given in the figure caption. These HTS results confirm the dose-dependent inhibitory effect of 2-APB on μTsunami-induced mechanosignalling (columns 1–4). Moreover, we find that neither PP2 nor Verapamil (columns 5 and 6) affect Ca^{2+} signalling. This is expected, as 2-APB is the only molecule tested known to be specific to ER Ca^{2+} release. Moreover the positive controls, which test Ca^{2+}-free media alone as well as the addition of DMSO (columns 10–12), demonstrate activation of cellular mechanotransduction. Interestingly, additions of cytochalasin-D or nocodazole (columns 7 and 8), which interfere with actin and microtubule polymerization, respectively, appear to have a mild inhibitory effect on μTsunami-induced Ca^{2+} signalling. Finally, the addition of blebbistatin (column 9) does not appear to interfere with μTsunami-induced Ca^{2+} signalling. The total time necessary to screen all 96 wells is constrained by the latency in the Ca^{2+} signalling dynamics (Fig. 3c), which requires us to image each well for 35 seconds following μTsunami exposure. This results in a total screening time of 56 min, a speed that is unprecedented for the completion of 96 independent mechanotransduction measurements, each of which assayed, on average, 36 cells in the annular region examined.

To secure our claim that the observed Ca^{2+} signalling is due to mechanotransduction, we must address the possibility that either: (i) cells are stimulated by cell lysate created near the bubble centre and transported to distal cells, or (ii) cells immediately proximal to the bubble are mechanically stimulated, while the Ca^{2+} signalling of cells located more distally is dependent on cell-cell contact. The second hypothesis is particularly relevant since the speed of our calcium wave is similar to that reported for a sheet of endothelial cells where only a single cell is mechanically stimulated by a micropipette tip[41]. To reject hypothesis (i), we must confirm that exposure to cell lysate alone is not responsible for the observed Ca^{2+} dynamics. To investigate this, we dosed cells with a solution of cell lysate (see Methods) immediately following Ca^{2+} signalling in response to μTsunami exposure. In addition, we exposed cells to cell lysate alone. As positive controls, we measured the Ca^{2+} signalling

response produced by ATP both following μTsunami stimulated signalling as well as without μTsunami exposure. As a negative control, we examined Ca^{2+} signalling without exposing the HUVECs to cell lysate, ATP or the μTsunami. While ATP elicited the expected Ca^{2+} signalling response, the administration of cell lysate consistently resulted in low levels Ca^{2+} signalling that was comparable to the negative controls and independent of μTsunami exposure (Supplementary Fig. 1). To directly test hypothesis (ii) we cultured HUVECs on glass-bottom Petri dishes that were patterned with fibronectin as shown in Supplementary Fig. 2a. The laser microbeam was delivered within a cell-free region that resulted in Ca^{2+} signalling in a population of cells immediately adjacent to the μCB as well as in a second distal region that was separated from the first by another cell-free zone (Supplementary Fig. 2b,c). This result demonstrates that the Ca^{2+} signals can propagate across regions free of cell-cell junctions leaving mechanotransduction as the primary mechanism of Ca^{2+} signalling in the second region. Therefore the observed cellular mechanotransduction does not rely on cell-cell contact throughout the entire cell culture.

Summary and Outlook

We have developed and validated a simple optical method that uses impulsive mechanical stimuli (μTsunamis) to discover molecules that regulate physiological signalling. Our method is capable of measuring downstream mechanosignalling in real time while maintaining sensitivity to the action of exogenous molecules. We have also demonstrated high-throughout screening of small molecules for their ability to affect cellular mechanotransduction via the combined use of pulsed laser microbeam irradiation and image cytometry. The instrumentation required for μTsunami generation can be easily integrated with commercial microscopes or imaging cytometers used in HTS via introduction of a focused low-energy laser beam into the optical path. The use of standard fluorescence microscopy to image calcium signalling provides a simple real-time readout of cellular mechanotransduction. Moreover, we envision that the use of multi-channel imaging will allow simultaneous measurement of other fluorescent molecules capable of probing mechanotransduction processes such as NO production, kinase activity (using genetically encoded FRET sensors[1,42]), and membrane potential.

Our μTsunami method eschews the use of pumps, actuators, and microfluidic technologies, any of which would encumber a rapid HTS approach. The compatibility of our method with standard image cytometry also makes this approach compelling for the study of mechanotransduction in standard 2-D cell cultures as well as 3-D tissue matrices within high-density well plates. The ability to use laser microbeam irradiation to form μCBs in 3-D tissue matrices has been reported and characterized[43]. In these systems, both adjustments to μCB size and ECM composition can expose cells to a broad range of viscous and elastic stresses. The application of laser-generated μCBs and fluorescent probes in 3-D tissue matrices can enable studies of the role of mechanotransduction in processes such as tumour growth and metastasis, traumatic brain injury, stem cell differentiation, and tissue development.

Methods

Shear stress computations

We use mass conservation in conjunction with the Gilmore model predictions for $R_B(t)$ and $V_B(t)$ to quantify the shear stresses. The Gilmore model assumes irrotational flow and applies mass and momentum conservation using a formulation that accounts for the effects of fluid inertia, viscosity, compressibility, and surface tension on the μCB dynamics. Specifically, we apply mass conservation to determine the time-resolved external fluid velocity $V_\infty(r,t)$ at any radial position r from the bubble centre larger than the maximum μCB radius R_{max}[38]. Momentum conservation is then applied, using the solution to Stokes first problem and Duhamel's superposition integral, to calculate the cellular exposure to time-resolved shear stress, $\tau(r,t)$[22,38]:

$$\tau(r,t) = \rho\nu\left(\frac{\partial V}{\partial z}\right)\Big|_{z=0} = \rho\sqrt{\frac{\nu}{\pi}}\int_0^t \frac{\partial V_\infty\left(r,t'\right)}{\partial t'}\frac{\mathrm{d}t'}{\sqrt{t-t'}},$$

where ρ and ν are fluid density and kinematic viscosity, respectively, $V(r, z, t)$ represents the spatial and temporal distribution of the fluid velocity and z=0 represents the horizontal cell surface (Fig. 2).

Laser microscope

μCBs were created using a Q-switched pulsed microchip laser (PNG-M03012, Teem Photonics) emitting 500 ps duration pulses at λ=532nm. The laser beam was expanded and collimated and the pulse energy was controlled using a λ/2 wave plate and polarizing beam splitter. An iris was used to select a central portion of the beam that was directed into an inverted microscope (Olympus IX-81) by a dichroic (Chroma ZT532NBDC) mirror. The beam was focused by a 20x, 0.45-numerical-aperture microscope objective (Olympus IX-81). The laser microbeam is focused 10 μm above the cell monolayer by adjusting the collimation of the laser beam prior to its entrance into the rear aperture of the objective. This enables the acquisition of fluorescent images that are in focus while also delivering the laser microbeam focal volume 10 μm above the image plane.

Fluorescence microscopy was performed on the same inverted microscope using epifluorescence illumination from a mercury short-arc lamp (X-Cite 120PC, Lumen Dynamics). The filter cube containing a 480/40 excitation, 535/50 emission, and 505 LP dichroic filters (Chroma) were chosen based on the fluorescent probe specifications. The fluorescence emission was imaged by a CCD camera (Hamamatsu ORCA R2) mounted onto the left side microscope port. Image acquisition was controlled using μmanager software[44].

Time resolved imaging of μCB dynamics was achieved using a gated ICCD camera (Stanford Computer Optics, 4Picos). Time resolved image illumination was provided by the fluorescence emission of a dye cell that was delivered at the desired time delay following the arrival of the pulsed laser microbeam to the cell culture. The dye cell was pumped by a Q-switched frequency-doubled Nd:YAG laser (Quantel Brilliant B). The dye cell emission was captured by an optical fibre and directed to the microscope condenser. A delay pulse

generator (BNC 575, Berkeley Nucleonics Corp.) controlled the timing between the laser, camera gate, and dye cell emission. An oscilloscope (TDS 2024, Textronix) was used to monitor the corresponding electronic signals.

Cell culture

Primary adherent human umbilical vein endothelial cells, HUVECs at passage 4 (P4) were cultured to confluence in EBM-2, supplemented with EGM-2 BulletKit (Lonza). The cells were cultured in 35mm, glass bottom culture dishes (#1.5, WPI) coated in fibronectin (Sigma).

Intracellular calcium probe loading and monitoring

HUVECs were loaded with Fluo-3/AM (Molecular Probes) a fluorescent reporter whose emission increases upon binding cytosolic Ca^{2+}. The cells were incubated in Hank's Balanced Salt Solution with ions (HBSS+) and 6 μM Fluo-3/AM for 45-60 min at room temperature, after which the cells were allowed to incubate for 15-30 min in EGM-2.

Immediately prior to experimentation, cells were rinsed with HEPES buffered Hank's Balanced Salt Solution without calcium supplemented with Mg^{2+} and 2 mg/mL D-glucose (HHBSS-) and 3 mM EGTA (Sigma) to chelate any remaining traces of extracellular calcium[45]. Cellular exposure to μCBs and imaging was performed at room temperature.

Ca^{2+} signalling agonist and inhibition

We administered ATP (50 μM, Sigma) to HUVEC cultures following μTsunami-induced Ca^{2+} signalling to confirm cellular responsivity to chemical stimulation of ER Ca^{2+} release. For the IP_3 inhibition experiments, we administered 10, 30, or 100 μM 2-Aminoethoxydiphenyl borate, (2-APB, Sigma) in 5% DMSO.

Cellular substrate patterning

Fibronectin was patterned in a pinwheel configuration on glass using a soft lithography protocol developed for ECM patterning[46,47].

Multi well plate preparation

Glass-bottom 96 well plates (#1.5, Invitro-Scientific) were coated with fibronectin and HUVECs plated in each well. Molecules added to wells were: 10 and 100 μM 2-APB, 10 μM PP2 (Sigma), 50 nM Verapamil (Sigma), 10μM cytochalasin D, 20 μM nocodazole, 20 μM blebbistatin, and 5% DMSO. 5% DMSO represents the highest concentration used as a solvent across all molecules tested.

Cell lysate preparation

HUVECs were grown to confluency in a T25 tissue culture flask, trypsinized and resuspended in standard HBSS- at a concentration of 1.5×10^7 cells/mL. Cell lysate was prepared by subjecting the cell solution to repeated freeze-thaw cycles at −80°C followed by sonication on ice for 30 s.

Supplementary Material

Refer to Web version on PubMed Central for supplementary material.

Acknowledgements

We thank Dr. Amy Hellman for her early contributions to this research, Prof. Michelle Khine for assistance with microfabrication and Prof. Christopher Hughes for supplying HUVECs. This research was funded through the Laser Microbeam and Medical Program, a National Biomedical Technology Resource (P41-EB015890) supported by the National Institutes of Health, the National Science Foundation through the Integrative Graduate Education and Research Traineeship (IGERT) Program (DGE-1144901), and UC Irvine through the I3 Award Program.

References

1. Wang Y, et al. Visualizing the mechanical activation of Src. Nature. 2005; 434:10401045.
2. Peyton SR, Raub CB, Keschrumrus VP, Putnam AJ. The use of poly(ethylene glycol) hydrogels to investigate the impact of ECM chemistry and mechanics on smooth muscle cells. Biomaterials. 2006; 27:4881–93. [PubMed: 16762407]
3. Kumar S, et al. Viscoelastic retraction of single living stress fibers and its impact on cell shape, cytoskeletal organization, and extracellular matrix mechanics. Biophys. Journal. 2006; 90:3762–73.
4. Discher DE, Janmey P, Wang Y. Tissue cells feel and respond to the stiffness of their substrate. Science. 2005; 310:1139–43. [PubMed: 16293750]
5. Ingber DE. Tensegrity: the architectural basis of cellular mechanotransduction. Annu. Rev. Physiol. 1997; 59:575–99. [PubMed: 9074778]
6. Chien S. Mechanotransduction and endothelial cell homeostasis: the wisdom of the cell. Am. J. Physiol. Heart Circ. Physiol. 2007; 292:H1209–24. [PubMed: 17098825]
7. Jaalouk DE, Lammerding J. Mechanotransduction gone awry. Nat. Rev. Mol. Cell Biol. 2009; 10:63–73. [PubMed: 19197333]
8. Orr AW, Helmke BP, Blackman BR, Schwartz MA. Mechanisms of mechanotransduction. Dev. Cell. 2006; 10:11–20. [PubMed: 16399074]
9. Ingber D. Mechanobiology and diseases of mechanotransduction. Ann. Med. 2003; 35:564–577. [PubMed: 14708967]
10. Hahn C, Schwartz MA. Mechanotransduction in vascular physiology and atherogenesis. Nat. Rev. Mol. Cell Biol. 2009; 10:53–62. [PubMed: 19197332]
11. Gottlieb PA, Suchyna TM, Ostrow LW, Sachs F. Mechanosensitive ion channels as drug targets. Curr. Drug Targets CNS Neurol. Disord. 2004; 3:287–95. [PubMed: 15379605]
12. Huh D, Hamilton GA, Ingber DE. From 3D cell culture to organs-on-chips. Trends Cell Biol. 2011; 21:745–54. [PubMed: 22033488]
13. Apic G, Ignjatovic T, Boyer S, Russell RB. Illuminating drug discovery with biological pathways. FEBS Lett. 2005; 579:1872–7. [PubMed: 15763566]
14. Drews J. Drug Discovery: A Historical Perspective. Science. 2000; 287:1960–1964. [PubMed: 10720314]
15. Rudin M, Weissleder R. Molecular imaging in drug discovery and development. Nat. Rev. Drug Discov. 2003; 2:123–31. [PubMed: 12563303]
16. Charras GT, Horton MA. Single cell mechanotransduction and its modulation analyzed by atomic force microscope indentation. Biophys. J. 2002; 82:2970–81. [PubMed: 12023220]
17. Chien S. Effects of disturbed flow on endothelial cells. Ann. Biomed. Eng. 2008; 36:554–62. [PubMed: 18172767]
18. Valberg PA, Butler JP. Magnetic particle motions within living cells. Physical theory and techniques. Biophys. J. 1987; 52:537–50. [PubMed: 3676435]
19. Chen CS, Mrksich M, Huang S, Whitesides GM, Ingber DE. Geometric control of cell life and death. Science. 1997; 276:1425–8. [PubMed: 9162012]

20. Shergill B, Meloty-Kapella L, Musse AA, Weinmaster G, Botvinick E. Optical tweezers studies on notch: single-molecule interaction strength is independent of ligand endocytosis. Dev. Cell. 2012; 22:1313–20. [PubMed: 22658935]
21. Meloty-Kapella L, Shergill B, Kuon J, Botvinick E, Weinmaster G. Notch ligand endocytosis generates mechanical pulling force dependent on dynamin, epsins, and actin. Dev. Cell. 2012; 22:1299–312. [PubMed: 22658936]
22. Rau KR, Quinto-Su PA, Hellman AN, Venugopalan V. Pulsed laser microbeam-induced cell lysis: time-resolved imaging and analysis of hydrodynamic effects. Biophys. J. 2006; 91:317–29. [PubMed: 16617076]
23. Hellman AN, Rau KR, Yoon HH, Venugopalan V. Biophysical response to pulsed laser microbeam-induced cell lysis and molecular delivery. J. Biophotonics. 2008; 1:24–35. [PubMed: 19343632]
24. Davies PF. Flow-mediated endothelial mechanotransduction. Physiol. Rev. 1995; 75:519–60. [PubMed: 7624393]
25. Tran QK, Watanabe H. Calcium signalling in the endothelium. Handb. Exp. Pharmacol. 2006; 2:145–87. [PubMed: 16999219]
26. Kuchan MJ, Frangos JA. Role of calcium and calmodulin in flow-induced nitric oxide production in endothelial cells. Am. J. Physiol. 1994; 266:C628–36. [PubMed: 8166225]
27. Palmer AE, Tsien RY. Measuring calcium signaling using genetically targetable fluorescent indicators. Nat. Protoc. 2006; 1:1057–65. [PubMed: 17406387]
28. Liu B, Lu S, Zheng S, Jiang Z, Wang Y. Two distinct phases of calcium signalling under flow. Cardiovasc. Res. 2011; 91:124–33. [PubMed: 21285296]
29. Vogel A, Venugopalan V. Mechanisms of pulsed laser ablation of biological tissues. Chem. Rev. 2003; 103:577–644. [PubMed: 12580643]
30. Vogel A, Noack J, Hüttman G, Paltauf G. Mechanisms of femtosecond laser nanosurgery of cells and tissues. Appl. Phys. B. 2005; 81:1015–1047.
31. Venugopalan V, Guerra A, Nahen K, Vogel A. Role of laser-induced plasma formation in pulsed cellular microsurgery and micromanipulation. Phys. Rev. Lett. 2002; 88:1–4.
32. Vogel A. Nonlinear absorption: intraocular microsurgery and laser lithotripsy. Phys. Med. Biol. 1997; 42:895–912. [PubMed: 9172266]
33. Stevenson DJ, Gunn-Moore FJ, Campbell P, Dholakia K. Single cell optical transfection. J. R. Soc. Interface. 2010; 7:863–71. [PubMed: 20064901]
34. Gilmore FR. The Growth or Collapse of a Spherical Bubble in a Viscous Liquid. Office of Naval Research. 1952
35. Knapp, RT.; Daily, JW.; Hammitt, FG. Cavitation. McGraw-Hill; New York: 1970.
36. Vogel A, Busch S, Parlitz U. Shock wave emission and cavitation bubble generation by picosecond and nanosecond optical breakdown in water. J. Acoust. Soc. Am. 1996; 100:148.
37. Vogel A, Linz N, Freidank S, Paltauf G. Femtosecond-laser-induced nanocavitation in water: Implications for optical breakdown threshold and cell surgery. Phys. Rev. Lett. 2008; 100:1–4.
38. Compton JL, Hellman AN, Venugopalan V. Hydrodynamic determinants of cell necrosis and molecular delivery produced by pulsed laser microbeam irradiation of adherent cells. Biophys. J. 2013; 105:2221–2231. [PubMed: 24209868]
39. Malek AM, Alper SL, Izumo S. Hemodynamic shear stress and its role in atherosclerosis. JAMA. 1999; 282:2035–42. [PubMed: 10591386]
40. Bishara NB, Murphy TV, Hill MA. Capacitative Ca(2+) entry in vascular endothelial cells is mediated via pathways sensitive to 2 aminoethoxydiphenyl borate and xestospongin C. Br. J. Pharmacol. 2002; 135:119–28. [PubMed: 11786487]
41. Demer LL, Wortham CM, Dirksen ER, Sanderson MJ. Mechanical stimulation induces intercellular calcium signaling in bovine aortic endothelial cells. Am. J. Physiol. 1993; 264:H2094–102. [PubMed: 8322938]
42. Seong J, Lu S, Wang Y. Live Cell Imaging of Src/FAK Signaling by FRET. Cell. Mol. Bioeng. 2011; 4:138–147. [PubMed: 21857884]

43. Cherian AV, Rau KR. Pulsed-laser-induced damage in rat corneas: time-resolved imaging of physical effects and acute biological response. J. Biomed. Opt. 2008; 13:024009. [PubMed: 18465972]

44. Edelstein A, Amodaj N, Hoover K, Vale R, Stuurman N. Computer control of microscopes using μManager. Current Protocols in Molecular Biology, edited by Frederick M. Ausubel et al. 2010 Chapter 14, Unit14.20.

45. Palmer AE, Tsien RY. Measuring calcium signaling using genetically targetable fluorescent indicators. Nat. Protoc. 2006; 1:1057–65. [PubMed: 17406387]

46. Park JW, Vahidi B, Taylor AM, Rhee SW, Jeon NL. Microfluidic culture platform for neuroscience research. Nat. Protoc. 2006; 1:2128–36. [PubMed: 17487204]

47. Yang MT, Fu J, Wang Y-K, Desai RA, Chen CS. Assaying stem cell mechanobiology on microfabricated elastomeric substrates with geometrically modulated rigidity. Nat. Protoc. 2011; 6:187–213. [PubMed: 21293460]

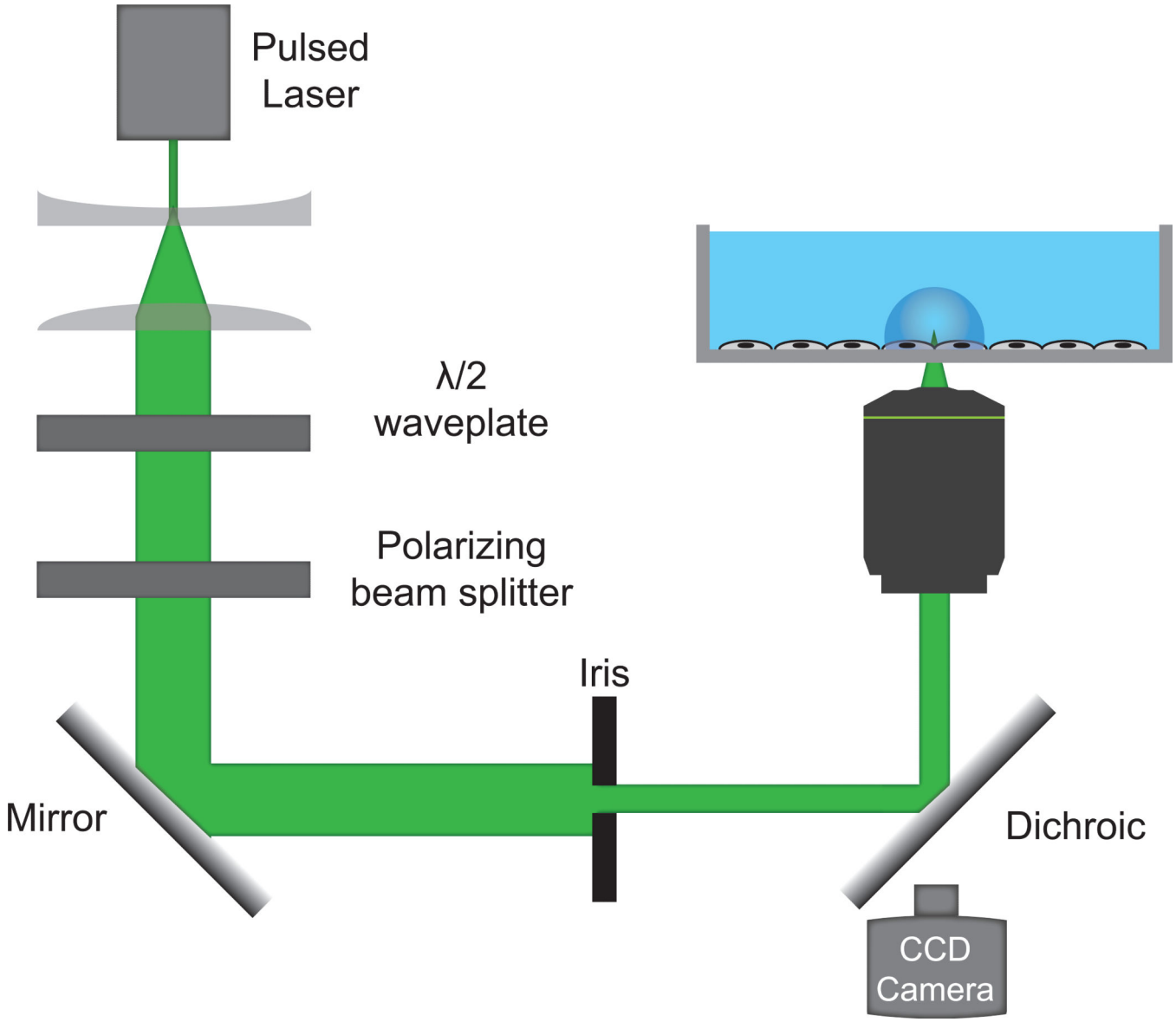

Figure 1. Pulsed Laser Microbeam exposes adherent cells to a transient μCB

A pulsed laser microbeam is integrated within an inverted fluorescence microscope and focused to a location ~10μm above cultured cells. Pulse energy is controlled using a half wave plate followed by a linear polarizer to control the pulse energy. Imaging is performed using a CCD camera.

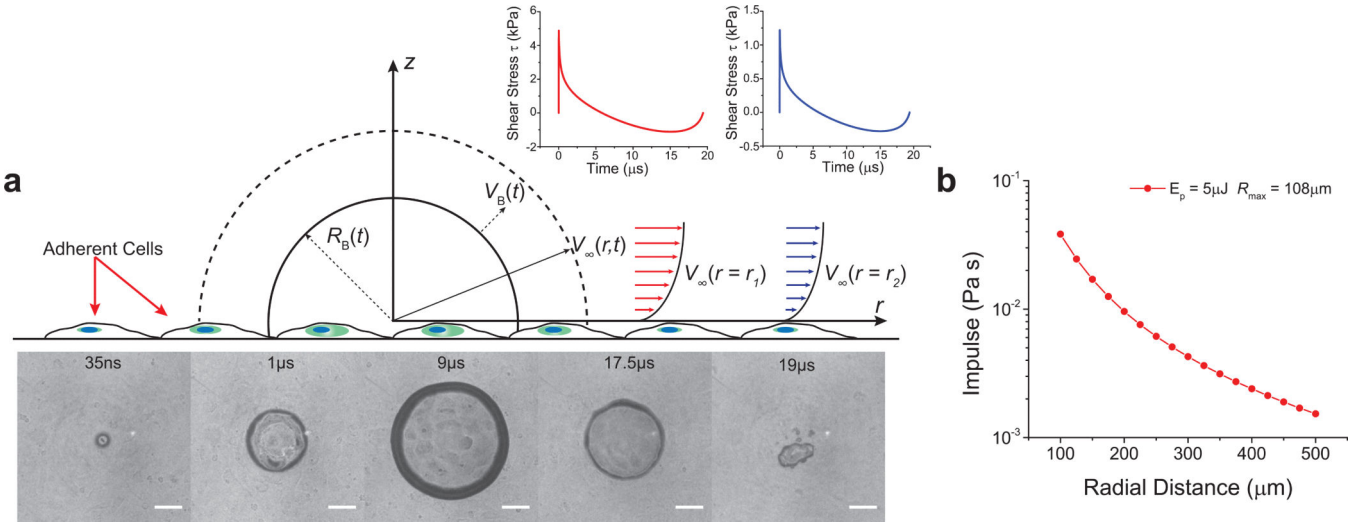

Figure 2. Radial dependence of μTsunami generated hydrodynamic shear stress impulse

(**a**) Schematic of a cross sectional view at time *t* through the centre of a μCB with wall radius, $R_B(t)$, and velocity $V_B(t)$. The surrounding fluid moves with velocity $V_\infty(r,t)$ in response to the μCB expansion and collapse. The image panel shows a time-resolved series of a single μCB (scale bar, 50μm), that reaches a maximum radius of R_{max}=108 μm in 9μs. This μCB was generated by a single 500ps laser pulse with 5 μJ pulse energy. The resulting fluid flow results in local transient shear stresses that decrease in amplitude with larger radial position. (**b**) Computed shear stress impulse for μCBs with R_{max} = 108μm.

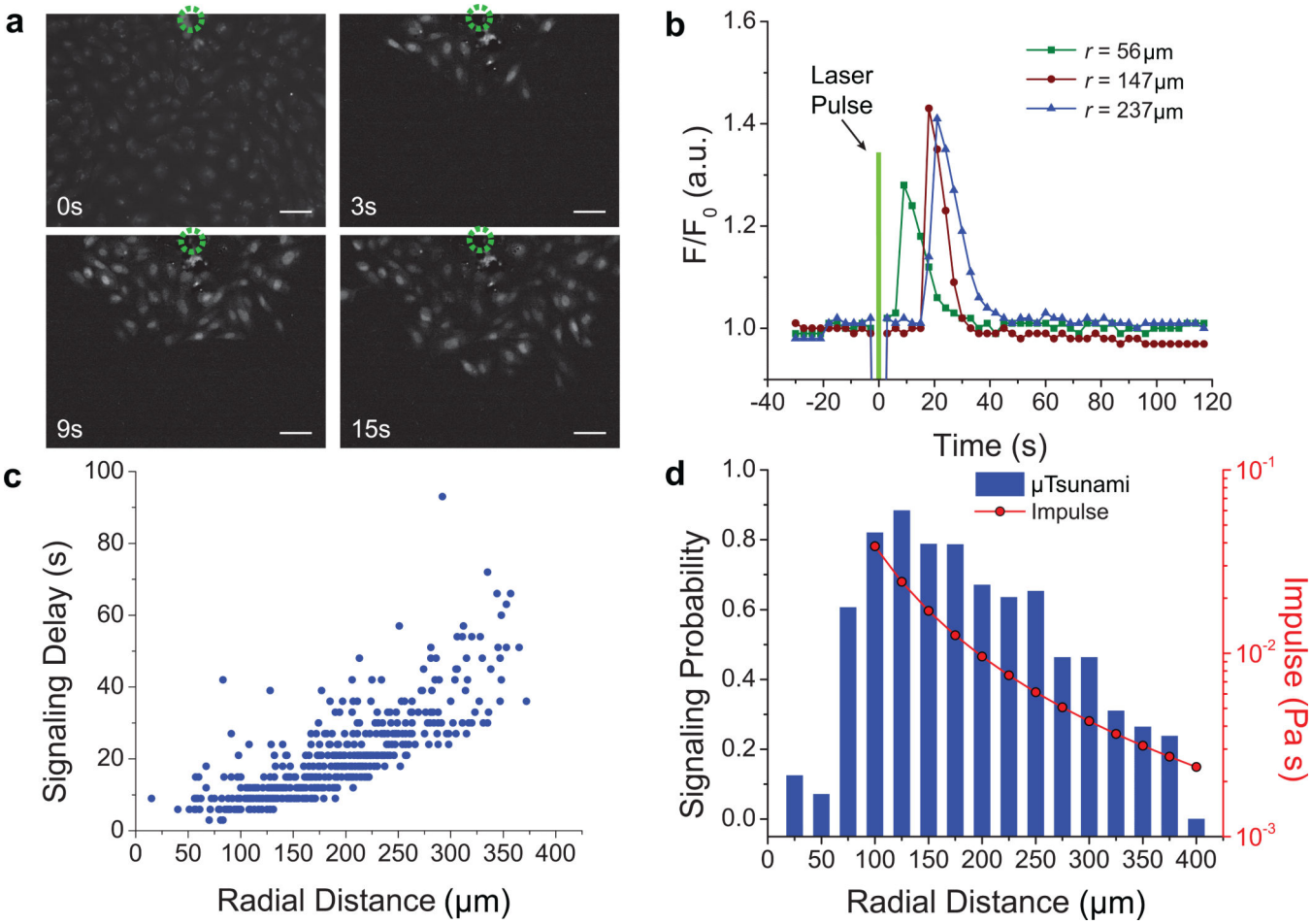

Figure 3. Calcium signalling following μTsunami exposure

(**a**) Fluorescence image time series of cytoplasmic calcium signalling in a confluent monolayer of HUVECs resulting from μTsunami exposure generated by a single 108μm diameter μCB. The green circle denotes the location of pulsed laser microbeam delivery immediately following the 0 sec time point. Subsequent images are displayed following background subtraction of the 0 sec image. Scale bar, 50μm. (**b**) Intracellular calcium-mediated fluorescence dynamics for three cells located at radial positions r = 56, 147, and 237μm from the μCB centre. Fluorescence intensities are normalized relative to the baseline intensity F_0. (**c**) Calcium signalling delay time versus radial distance from the μCB centre for 447 cells that signal out of 765 cells monitored in five separate experiments. (**d**) Ca^{2+} signalling probability and shear stress impulse versus radial distance from the μCB centre.

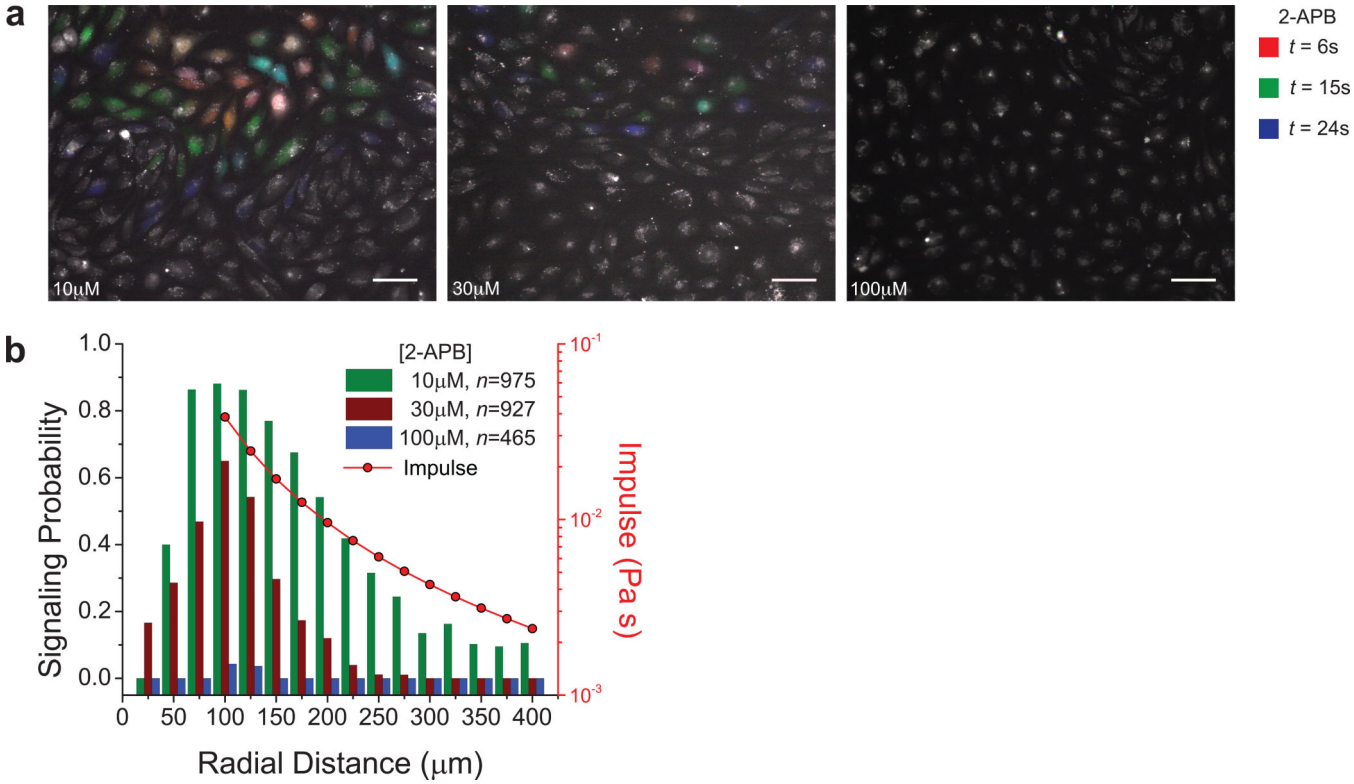

Figure 4. Dose dependent effect of IP_3 inhibitor on μTsumani-induced calcium signalling

(**a**) Fluorescence images (Fluo-3/AM) of μCB generated calcium signalling following incubation in 10, 30 or 100 μM 2-APB. To depict the propagation dynamics of the calcium signalling we mapped time to color as (red: *t* = 6s, green: *t*=15s, blue: *t*=24s). Scale bar, 50 μm. (**b**) Calcium signalling probability decreases with increasing 2-APB concentration.

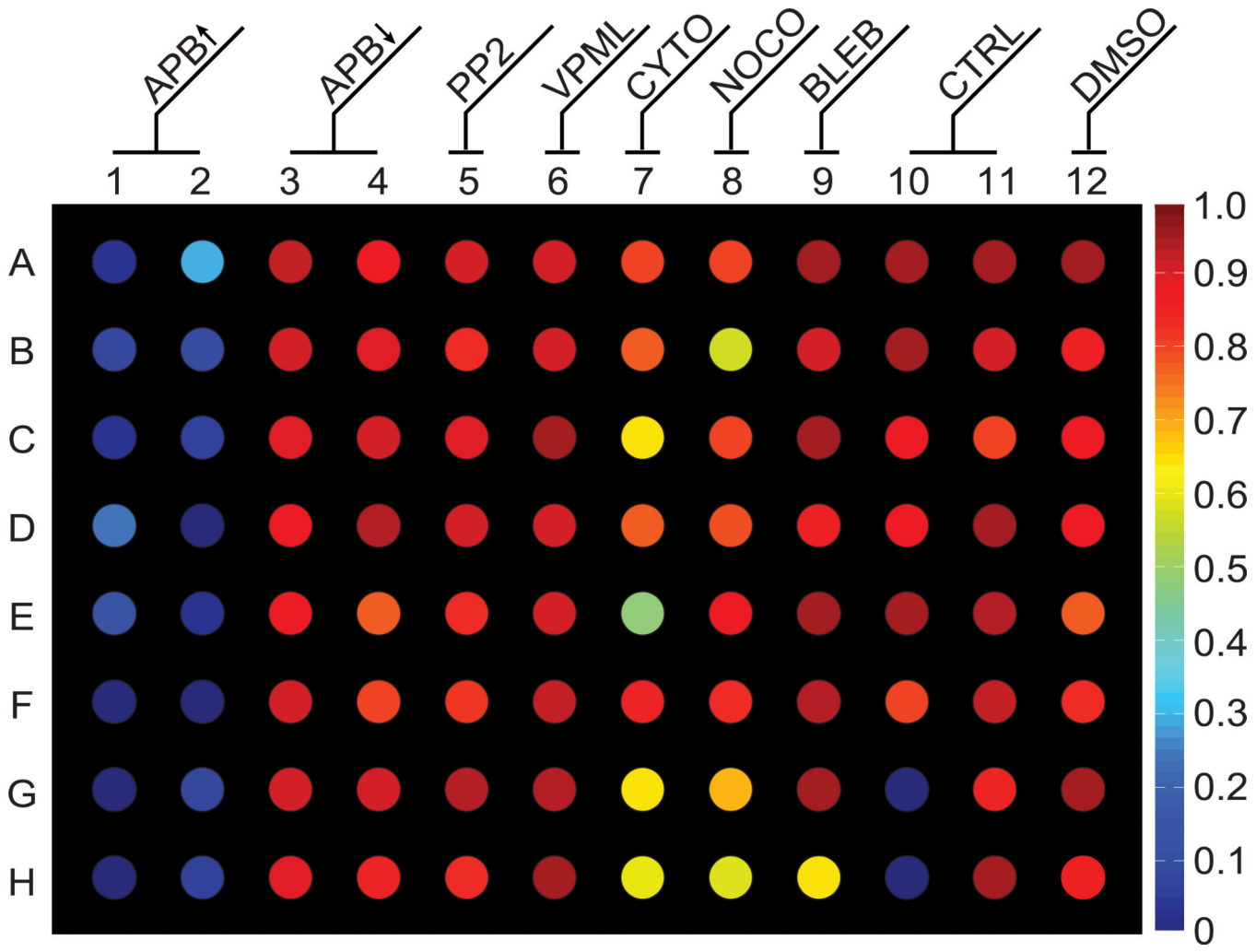

Figure 5. Use of μTsunamis for HTS

Results of a 96 well plate screen for μTsunami-induced Ca^{2+} signalling in HUVECs in the presence of exogenous molecules. Each of the 12 columns has 8 replicates. The contents of the twelve columns are as follows: 1,2: 100 μM 2-APB, 3,4: 10 μM 2-APB, 5: 10 μM PP2, 6: 50 nm Verapamil, 7: 10 μM Cytochalasin-D, 8: 20 μM Nocodazole, 9: 20 μM Blebbistatin, 10,11: Control, 12: 5% DMSO. Cells within an annulus spanning 100-150μm from the centre of μCB were used to determine the results of calcium signalling in each well. The colour of each well corresponds to the percentage of these cells that signalled. The median percentage of cells that display Ca^{2+} signalling in each of the columns (1-12) = [3, 6, 94, 93, 91, 96, 75, 84, 99, 92, 98, 91]%.